Materials Research. 2023; 26(suppl. 1):e20230056
DOI: https://doi.org/10.1590/1980-5373-MR-2023-0056

K_{Ic} Determination of a 7075 T6 Aluminum Alloy by Critical Distances Theory and LEFM

***Larissa Gomes Simão*[a*], *Eduardo Atem de Carvalho*[a]**

[a]*Universidade Estadual do Norte Fluminense (UENF), Laboratório de Materiais Avançados (LAMAV), Campos dos Goytacazes, RJ, Brasil.*

Received: January 16, 2023; Revised: April 12, 2023; Accepted: May 28, 2023

The Critical Distances Theory has been used in engineering field as a less expensive method to predict failures. Thus, this research aims to evaluate its methods in other materials, like the aluminum alloy 7075 T6, and notches. Two different notches were machined: a sharp and a blunted, with radius of 0,025 mm and 0,045 mm, respectively. The first in specimens of tests tension and the last in bend tests specimens. The DCT methods analyzed exhibited low percent differences and predictions mutually consistent. However, the Line Method stood out when presented 3% to percent difference. The analysis to stress field around of sharp notch tip, LM achieved a value of 12 MPa√m para K_{Ic}. Although, when these same results were applied in the Traditional Fracture Mechanics equations, a fracture toughness of 34 MPa√m was found. This last result is one of the best predictions achieved until the present moment in this research group. Mainly when compared with other works which determined the same property using the same thermal treatment conditions to this alloy.

Keywords: *Critical Distances Theory, AA 7075 T6 Aluminum Alloy, Artificial Aging, LEFM.*

1. Introduction

Among the fields of interest in Fracture Mechanics, it is found failure prediction[1]. Both flaws caused by design or service are potential crack initiators which may cause material failure. Therefore, it is not surprising that these singularities are central to the research field. But, notches, much easier found in structures and simulated in test rigs, have gained attention since cracks may propagate for their roots[2].

In parallel to this, simply following of standards for correct materials properties determination, such as K_{Ic}, is advisable. But, according to Taylor and Susmel in their works, application of available technics demands sofisticated equipments and a certain level of expertise. Testing is time consuming and costly, if following ASTM E399[3], for example. This tends to be outside the possibility of small research groups in academia.

In this context, CDT finds its relevancy once it proposes, among other things, to predict failure loads under acceptable error, if one considers Linear Elastic Fracture Mechanics predictions, and for a fraction of the cost of the standard methods. Some authors consider CDT as a settled theory, but Taylor himself[4] in the latest papers proposes that new works are to be made to confirm and evaluated DCT vis a vis other Fracture Mechanics theories[5].

Therefore, this work tested the reliability of two methods proposed by Critical Distances Theory (CDT). Its predictions were matched against those made by classic Linear Elastic Fracture Mechanics (LEFM), in order to searching for a class of theories aiming Fracture Strength determination at low cost utilizing a well-known industrial metal alloy, AA 7075 T6.

Aluminum presents excellent machinability, a desirable property in research field, considering low cost for specimen fabrication, as compared to steel[6]. Among aluminum alloys, AA 7075 T6 is one of the most used ones and the ablest to suffer age hardening[7]. This 7XXX series alloy, in which zinc is the principal alloying element, presents high mechanical strength and excellent ductility, fracture toughness and fatigue strength[8].

Once that weight reduction is one crucial aspect of aircraft design[9], recent prognosis programs for aging military aircraft have revived research on high strength 7075-T6 series aluminum alloys that have been used as structural materials for airframes[10]. This alloy plays an irreplaceable role in the Aviation Industry field, such as aircraft wing panel, wing beam, wing rib, and fuselage internal support components[11]. Moreover, there is an increasing demand for the use of age hardenable alloy within the Automotive Industry, due to its advantages of high strength-to-weight ratio, good corrosion resistance and formability[12]. Hence, aluminum alloys are gaining increasing use in the construction industry, underpinned by extensive research[13]. Specialists indicate it like key structural materials in modern transportation[14], confirming relevance of the selected material.

Besides that, to test a particular aspect of the so-called Critical Distances Theory (CDT), it is advisable to employ a material which properties are well known and readily available.

1.1. The Critical Distances Theory (CDT)

In general, the CDT proposes that the failure of a body containing a stress concentration, crack or notch, can be predicted using elastic stress information in a critical region close to the notch tip. Therefore it may be considered a LEFM extension. The standard LEFM approach requires the knowledge of one characteristic parameter, K_c, CDT,

*e-mail: simao_larissa@yahoo.com.br

in other hand, requires also a second parameter, L, named characteristic length[15] and may be determined by Equation 1:

Equation 1:

$$L = \frac{1}{\pi}\left(\frac{K_{I_c}}{\sigma_0}\right)^2$$

Where K_{1c} is the fracture toughness and σ_0 is the material's inherent strength.

CDT take as departuring point that failure may be averted as long as effective stress, σ_{eff}, is smaller than the inherent strength, σ_0, a material-dependent property[4].

There are 4 CDT methods. They are: Line Method, Point, Area and Volume. The two latest ones are outside the focus of this work, thus they will not be covered.

The Line Method (also known as the Average Stress Criteria) stablishes that failure in any given component happens when linear elastic effective stress σ_{eff}, ahead of a notch reaches an average value along a line of 2L length equals to the material's inherent strength, σ_0 (Figure 1a)[4].

Few years later, the Line Method (LM), postulated by Neuber[16] was simplified by Peterson[17], adding an observation that the effective stress could be determined at a given distance from the notch root (Figure 1b).

Therefore, the Point Method (PM), also known as the Maximum Stress Criteria, considers that the failure of a component under statically loading happens when effective stress, σ_{eff}, reaches the value of the inherent strength, σ_0, at a distance L/2 from the notch root (Figure 1b).

Both methods, Point and Line, may be expressed as it follows, in Equations 2 and 3, respectively:[4]

Equation 2:

$$\sigma_{eff} = \sigma_1\left(\theta = 0, r = \frac{L}{2}\right) = \sigma_0$$

Equation 3:

$$\sigma_{eff} = \frac{1}{2L}\int_0^{2L} \sigma_1\left(\theta = 0, r\right) dr = \sigma_0$$

2. Experimental Procedure

2.1. Heat treatment

A commercial AA 7075 T6 alloy was chosen for this study. Two shapes were adopted: a round bar and a plate. Both shapes were solubilized between 460 and 499 °C. Afterwards, they were quenched into a water, salt and ice solution (at around 0 and 5 °C), and finally aged artificially at 121 °C during 24 h[18]. Given the different thicknesses of the shapes, different times at a given temperature were selected. The circular bar was solubilized for 1 h 10 min and kept for 1 h at quenching temperature. The plate was solubilized for 2 hours and kept at quenching temperature for 1 h 10 min[18].

2.2. Machining

Standard tensile specimens with and without notch were machined from the round bar. The bending specimens were cut from the plate. Tensile specimens without notch[19] were utilized for the necessary required by CDT mechanical properties determination, such as Young's Modulus, Yielding Strength, Ultimate Strength and Strain. Poisson's Ratio was taken from the references. Notched specimens were used for CDT methodology application and two different ones were machined: a sharp one, present in the tensile specimens and a blunt one, used in the bending specimens. The radius were 0.025 mm and 0.045 mm, respectively. All other dimensions are listed in Figure 2 and 3. The same dimensions, after metrological evaluation, were used by the Finite Element model to determine stress levels.

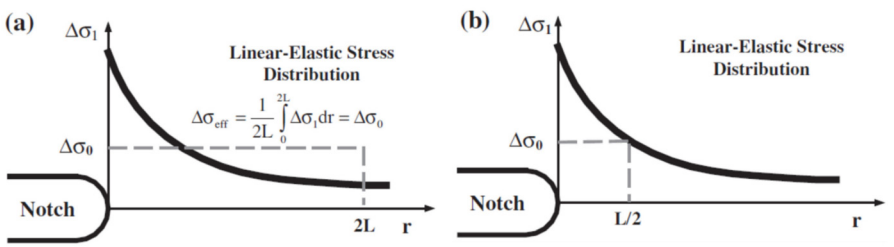

Figure 1. CDT methods used in this work: (a) Line Method, and (b) Point Method[7].

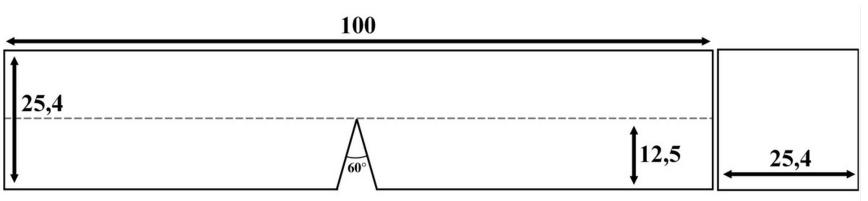

Figure 2. Bending specimen dimensions. All dimensions in millimeters.

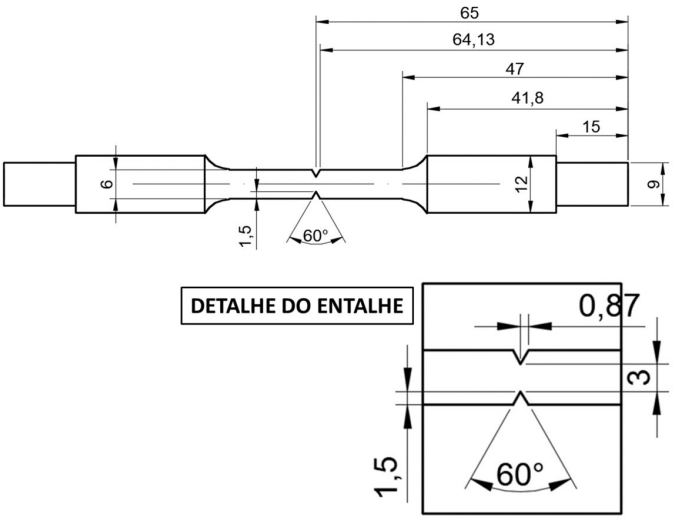

Figure 3. Tensile specimen dimensions, according to ASTM E8 standard[19], but with a circular notch. All dimensions in millimeters.

2.3. Finite elements modeling

For near-tip stress field analysis, two Finite Element models were developed. The first, for a v-notched, four-point bending, prismatic specimen. The second model represented the circular, v-notched tensile specimen.

Both models were submitted to the fracture loads and other properties previously determined. ANSYS version 19.2 software was used and PLANE183 elements were chosen. This element is commonly used for bidimensional solid structures, and it is defined by four nodes and two degrees of freedom.

2.4. Breaking loads determination

Considering an already mentioned reference[4] parameters, all tests related to notched specimens were performed. Tables 1 and 2 present, respectively, list the breaking loads gathered at the tensile tests (0.025 mm notch root radius) and four-point bending, 0.045 mm notch root radius specimens.

The average rupture load (from Tables 1 and 2), together with mechanical properties taken from tensile tests (Table 3) were supplied to the respective Finite Elements models, and the stress field ahead of the notches were therefore determined.

2.5. CDT application - point method

Finite Element generated stress fields were plotted for both notches types at the same graphic and scale and Figure 4 was generated.

According to the Critical Distances Theory, for Point Method, the coordinate coinciding with the intersection point between the plotted curves yields the inherent stress at the ordinate axis, and at the abscises the ratio for the characteristic length L and 2, L/2, as indicated in Figure 1.

The CDT parameters for both notches are displayed at Table 4.

Values determined in this way were applies directly into the expressions predicting the theoretical Stress Intensity Factor adjusted for the Point Method[4].

Table 1. Rupture loads for the tensile test specimens, 0.025 mm notch root radius and 6 mm diameter.

	Load (N)
SPC1	12176
SPC2	13558
SPC3	13842
SPC4	12427
Average	**13001**
SD	**712**
VC	**5,48%**

Table 2. Rupture loads for the four-point bending, 0.045 mm notch root radius and 25.4 mm thickness.

	Load (N)
SPC1	57345
SPC2	56544
SPC3	55710
SPC4	*
Average	**56533**
SD	**667**
VC	**1,18%**

Note: *Non-valid test.

Equation 4:

$$K_c^{Theoretical} = \frac{\sigma_0\sqrt{\pi(\rho+L)}}{1+\frac{\rho}{\rho+L}}$$

Where ρ is the notch root radius.

The Experimental Stress Intensity Factor was determined by Creager and Paris' equation of the proposed $K_c^{Theoretical}$ changed by Taylor for CDT methods[20].

Table 3. AA 7075 T6 mechanical properties.

	σ_y (MPa)	σ_u (MPa)	E (MPa)	ε_{uv}	AR (%)
SPC1	578	621	62303	0,1173	17
SPC2	582	623	63836	*	21
SPC3	554	602	65509	*	14
SPC4	581	622	63816	*	17
Average	**574**	**617**	**63866**	-	**17**
SD	**13**	**10**	**1310**	-	**3**
VC	**0,02%**	**0,02%**	**0,02%**	-	**0,15%**

Note: *sensor failure precluded data collection

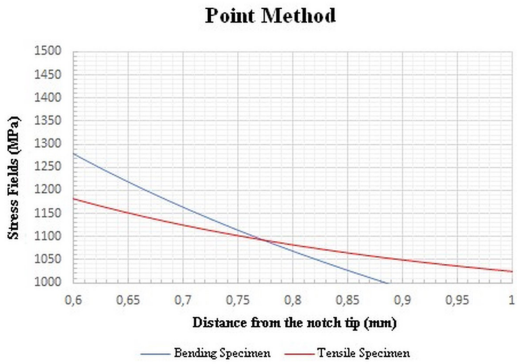

Figure 4. Stress fields versus Distance from notch root graphic, for both types of specimens.

Creager and Paris' expression (Eqn 5) take into account not an inherent stress, such Taylor did, but an effective stress at a null distance from the notch root (r = ρ/2, θ = 0). This stress may be assumed to be the one determined by FEM analysis at the same position.

Also, $K_c^{Theoretical}$ the axis origin, r, for the Experimental SIF is half of the size of the notch root radius ρ (r = ρ/2), so the origin does not match the notch tip. Results for $K_c^{Theoretical}$ and the theoretical predictions are listed in Table 5.

Equation 5:

$$K_c^{Exp} = \frac{\sigma_{\theta\theta}(r)\sqrt{2\pi r}}{1+\frac{\rho}{2r}}$$

The percentage difference was calculated using Equation 6, which validates the experimental data[21].

Equation 6:

$$Diff\,(\%) = \frac{Experimental\ SIF - Estimated\ SIF}{Estimated\ SIF}.100$$

2.6. CDT application - line method

As in Point Method, the stress generated fields simulated by Finite Elements were also graphed, but differently from previous methodology, the Line Method uses area below plotted curve calculation for each different notch, as specified by Equation 3. It can be seen that it is not a trivial graphic analysis, such as in Point Method.

Table 4. CDT parameters as determined by Point Method.

Inherent Stress, σ_0 (MPa)	Notch Root Distance, L/2 (mm)	Characteristic Length, L (mm)
1092	0,78	1,55

Table 5. Theoretical and Experimental predictions for Point Method.

ρ (mm)	$K_c^{Theor.}$ (MPa)	$K_c^{Exp.}$ (MPa)	Difference (%)
0,025	76	64	16
0,045	75	85	13

Table 6. CDT parameters determined by Line Method.

Inherent Stress, σ_0 (MPa)	Notch Root Distance, 2L (mm)	Characteristic Length, L (mm)
7009	0,04	0,02

Once this is understood, a sequence of steps is taken for the application of this CDT method:

- As stress and position points, as determined by FEM, are graphed (Figures 5a and b);
- A polynomial curve-fitting method was applied and the curve with the highest R^2 was selected;
- The polynomial was integrated.
- The integrated polynomials were equaled and a common point between curves was determined, a required CDT parameter determination procedure.
- The real roots were replaced into the integrated polynomials and the resulting area determined 2L.
- Once 2L is known, this value was replaced into Equation 7.
- Once the results converged, the inherent stress, σ_0, and characteristic length L, were calculated and are listed in Table 6.

The determined values were then applied to the equations for the Theoretical SIF prediction adjusted, this time, to the Line Method[4].

Equation 7:

$$K_c^{Theoretical} = \frac{2\sqrt{2\pi}.\sigma_0.L}{2\sqrt{\frac{\rho}{2}+2L} - \frac{\rho}{\sqrt{\frac{\rho}{2}+2L}}}$$

The Experimental Stress Intensity Factor was determined by Equation 5, from Creager and Paris.

The percentage of difference was calculated using expression 6.

3. Results and Discussion

3.1. Standard tensile test

Table 3 contains some mechanical properties extracted from the tensile test performed at an Universal Testing Machine Instron[19]. The values of Yield Strength and Ultimate Strength are higher, although still close to the reference values found in the literature: 505 MPa[8] and 490 MPa[22] for Yield Strength; 570 MPa[8] and 559 MPa[22] for Ultimate Strength and 72 GPa[8] for Young Modulus (to which the result found was inferior). The before mentioned references were selected considering the temperatures used for heat treatment. However, it is common knowledge that not only temperature parameters, but also other external conditions affect final properties. Nevertheless, the reference values are themselves scattered. Given the material's character, other properties are within the expected range, as well.

3.2. Finite elements modeling

Figures 6 a and b represent total strain for both types of specimens, under the average load determined experimentally for their fracture and Figures 7a and b show the stress field near the notch, for the above loading.

3.3. Critical Distances Theory method application

3.3.1. Point method

Results found for theoretical prediction in both cases, by Point Method, are presented in Table 5.

As it may be observed, the Point Method predicts theoretically, through $K_c^{Theoretical}$, the value for the Experimental SIF for the alloy AA 7075 T6, within the range of 15% difference. Similar values were found by Taylor in his works using other materials.

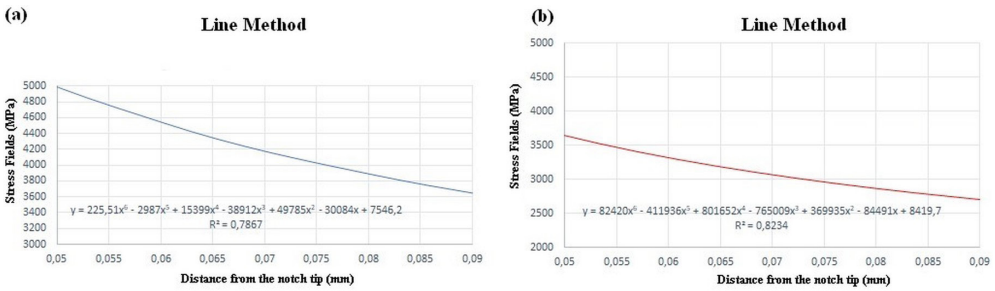

Figure 5. Stress fields versus Distance from the notch tip (a) for bending model with ρ = 0,045 mm and (b) tensile model with ρ = 0,025 mm.

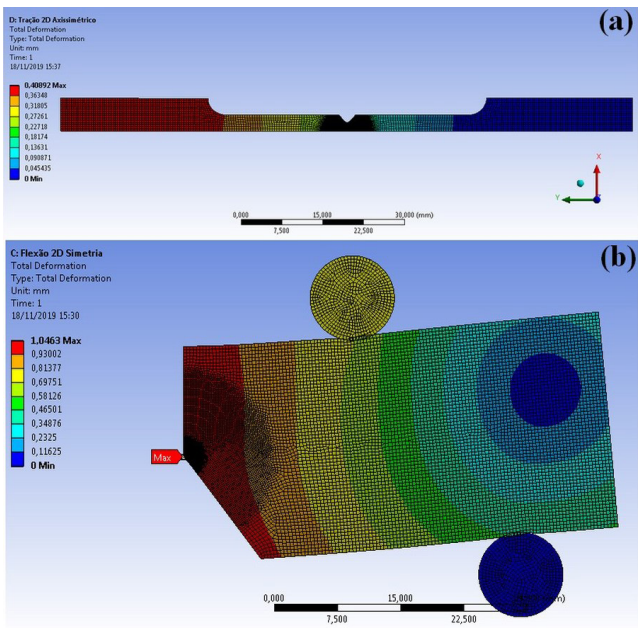

Figure 6. Total strain for the notched specimen (a) and for notched bending specimen (b).

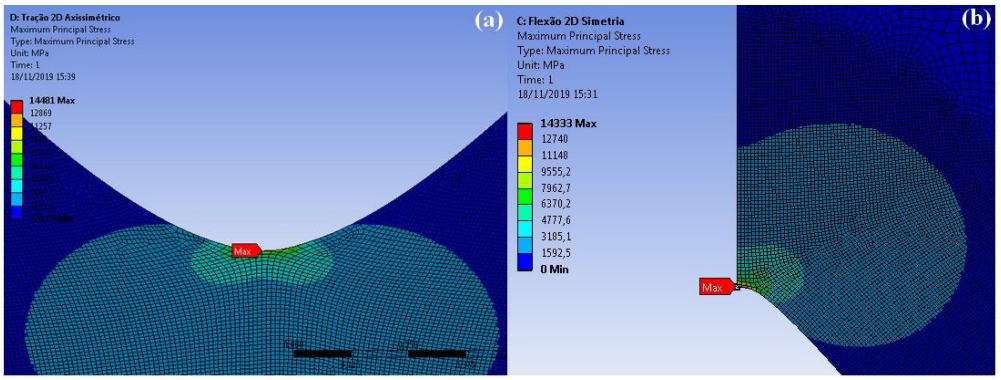

Figure 7. Near tip stress field zoom image taken from the 0.025 mm radius specimen analysis (a). Same for the 0.045 mm radius bending specimen (b).

Although these results may not be satisfactory by some standards, it is worth to remember that the CDT was derived taking into account just a Linear Elastic Zone, therefore, it is somehow a surprise that such a small difference was found between the theoretical and experimental predictions, considering that the studied alloys is by all means a ductile material.

Before going any further there is a necessity of analyzing the same stress fields, but now employing the Line Method.

3.3.2. Line method

The determined results for the theoretical prediction, both types of notches and Line Method, are presented in Table 7.

Unexpectedly, once most of works in this subject tend to find that Point Method yields the best results, it was found an even smaller difference if Line Method is applied to the sharp notch. For the blunted notched bending specimen concurs with the majority of works and Line Method displays a larger difference.

CDT parameters, characteristic length L, and inherent strength σ_0, found by both methods (Line and Point) were also applied to Equation 1, rearranged now in Equation 8. K_{Ic} for each method are listed in Table 8.

Equation 8:

$$K_{Ic} = \sigma_0 \sqrt{\pi L}$$

Values keep matching K_c determined by CDT methods, but when compared to those found in the literature the above values are higher, as it can be seen in Table 9.

Once K_{Ic} suffers direct influence of loading orientation given the anisotropic nature of the studied material, produced by machining, cold lamination and heat treatments, it is worth notice that value listed by Farahmand[24] was selected taking into account load and lamination direction, and crack growth path.

Table 9 shows that although CDT yields similar results between methods, mainly Line Method applied to case where notch radius was 0,025 mm (3%), in general it was not able to predict K_{Ic} satisfactorily.

Line Method results were the closest to those listed in Table 9.

Table 7. Theoretical and Experimental predictions for Line Method.

ρ (mm)	$K_c^{Theor.}$ (MPa)	$K_c^{Exp.}$ (MPa)	Difference (%)
0,025	62	64	3
0,045	62	85	38

Table 8. K_{Ic} as calculated by Point and Line Methods for AA 7075 T6 Aluminum Alloy.

CDT Method	$K_{Ic}\ (MPa\sqrt{m})$
Point	76
Line	54

Table 9. K_{Ic} according to the references listed for AA 7075 T6.

Source	$K_{Ic}\ (MPa\sqrt{m})$
ASM[8]	20 – 25
Callister[23]	24
Farahmand[24]	28
Cavalcante[7]	32

Considering the low R^2, that is indicated in the graphic of the Figure 5a and b, the solution was to restrict the points and, as expected, the curve-fitted polynomials for the stress fields presented high R^2.

The curve-fitting process ability to describe almost to perfection the stress field (R^2) was attained for the blunt and sharp notches, reaching 0.9994 and 0.9977 respectively. This is achieved by selecting the points placed the nearest to the notches and not using all points for the fitting process. As the parameters were applied to Equation 8, for K_{Ic} by Line Method determination, a 12 MPa√m is found. Although still far from available reference values (Table 9), the use of nearest to the notch points only yielded a more reasonable value than previously. This fact must be researched further

and does not belong in this present one, once ductile materials represent the biggest challenge to CDT.

3.4. Classic LEFM expressions comparison

It was noticed that the use of classical, Irwin, LEFM expressions yielded the best of all results, for the smallest radius. For the tensile, v-notched, specimen (ρ = 0,025 mm), Tada's equation[25] was used.

Equation 9:

$$K_I = \sigma_{net}\sqrt{\pi a}F_1\left(\frac{a}{b}\right)$$

Where σ_{net} (Equation 10) take into account the net ligament area only.
Equation 10:

$$\sigma_{net} = \frac{F}{\pi a^2}$$

Where F is the average rupture load, determined by all the specimens, a is the net ligament radius and b is the total section radius. All values were measured by a confocal microscope. The correction functions F(a/b) and G(a/b) are determined by Equations 11 and 12, respectively.
Equation 11:

$$F_1\left(\frac{a}{b}\right) = G\left(\frac{a}{b}\right)\sqrt{1-a/b)}$$

Equation 12:

$$G\left(\frac{a}{b}\right) = \frac{1}{2}\left\{1+\frac{1}{2}\frac{a}{b}+\frac{3}{8}\left(\frac{a}{b}\right)^2 - 0,363\left(\frac{a}{b}\right)^3 + 0,731\left(\frac{a}{b}\right)^4\right\}$$

For the "V" notched bending specimen (ρ = 0,045 mm), Equation 13[25] was used.

Equation 13:

$$K_I = \sigma\sqrt{\pi a}F\left(\frac{a}{b}\right)$$

Where a is the notch depth, and b is the total high. Equation 14 shows the nominal stress expression.
Equation 14:

$$\sigma = \frac{6M}{tb^2}$$

Where t is the specimen thickness. And for the four-point bending moment, Equation 15.
Equation 15:

$$M = \frac{F\left(L_2 - L_1\right)}{4}$$

Where F is the rupture load, L_2 and L_1 are the distances between the lower and upper rollers.

Equation 16:

$$F\left(\frac{a}{b}\right) = 1,122 - 1,40\left(\frac{a}{b}\right) + 7,33\left(\frac{a}{b}\right)^2 - 13,08\left(\frac{a}{b}\right)^3 + 14\left(\frac{a}{b}\right)^4$$

Table 10. K_{Ic} estimated for both specimens and AA 7075 T6.

Notch tip radius (mm)	K_{Ic} ($MPa\sqrt{m}$)
0,025	34
0,045	63

Table 10 shows the results reached by the above expressions use.

As it can be seen, Irwin's LEFM expressions are able to predict fairly well the material failure for the sharp notch, once the K_{Ic} is close to that found by Cavalcante[7], using classical standard fracture strength tests (Table 9), for the same aluminum alloy. In other hand, for the larger radius, obtained results are close to those yielded by CDT, showing the convergence between methods and formulations.

Besides the fact of the two different radiuses used, the specimens and loadings are also different, which may account for the listed values mismatch.

It must also be reported that confocal microscopy detected small irregularities in the region where the cutting bit exited the bending specimen. It may have added some degree of dispersion to the obtained results and somehow contaminated some results, but this was not confirmed nor denied by statistical analysis.

4. Conclusions

Point Method presented, for both notches, differences below 15%. But could not predict accurately K_{Ic}. This indicates that CDT requires further development until be able to handle ductile materials. On the other hand, Line Method has yielded a lower that 3% different between $K_c^{Theoretical}$ and K_c^{Exp}, for the stress field close to the sharp notch analysis. The analysis must be performed over the notch root near vicinity and yielded a K_{Ic} = 12 MPa√m.

Finally, the direct application the 0,025 mm radius and test parameters to LEFM expressions indicated a K_{Ic} = 34 MPa√m for the studied alloy. The same calculations (using different LEFM expressions) for the bending specimen failed to produce an acceptable result.

5. Acknowledgments

Capes – Coordenação de Aperfeiçoamento do Pessoal do Ensino Superior, for sponsoring the first Author scholarship.

6. References

1. Anderson TL. Fracture mechanics: fundamentals e applications. 3rd ed. Boca Raton: Taylor & Francis Group; 2005.
2. Taylor D. The theory of critical distances. Eng Fract Mech. 2007;75(7):1696-705.
3. ASTM: American Society for Testing and Materials. ASTM E399: standard test method for linear-elastic plane-strain fracture toughness of metallic materials. West Conshohocken: ASTM; 2022.
4. Susmel L, Taylor D. On the use of the Theory of Critical Distances to predict static failures in ductile metallic materials containing different geometrical features. Eng Fract Mech. 2008;75(15):4410-21.
5. Terra RVA. Avaliação da tenacidade à fratura real e do uso da teoria da distância crítica em materiais semi-frágeis. [dissertação]. Campos dos Goytacazes: Programa de Engenharia e Ciência

dos Materiais, Universidade Estadual do Norte Fluminense Darcy Ribeiro; 2013.
6. ABAL: Associação Brasileira de Alumínio. Fundamentos e aplicações do alumínio. São Paulo: ABAL; 2007.
7. Cavalcante FF. Comportamento mecânico e tenacidade à fratura de ligas de alumínio 2024 e 7075 submetidas a diferentes tempos de envelhecimento [dissertação]. Natal: Programa de Pós-graduação em Ciência e Engenharia de Materiais, Universidade Federal do Rio Grande do Norte; 2016.
8. ASM International. Handbook ASM. Heat treating. Materials Park, Ohio: ASM International; 2004. v. 4.
9. Liao Y, Li Y, Pan Q, Huang M, Zhou C. Residual fatigue life analysis and comparison of na aluminum lithium alloy structural repair for aviation applications. Eng Fract Mech. 2018;194:262-80.
10. Xue Y, McDowell DL, Horstemeyer MF, Dale MH, Jordon JB. Microstructure-based multistage fatigue modeling of aluminum alloy 7075-T651. Eng Fract Mech. 2007;74:2810-23.
11. Gao Z, He Y, Zhang S, Zhang T, Yang F. Research on corrosion damage evolution of aluminum alloy for aviation. Appl Sci. 2020;10:7184.
12. Wang X, Guo M, Cao L, Luo J, Zhang J, Zhuang L. Effect of heating rate on mechanical property, microstructure and texture evolution of Al-Mg-Si-Cu alloy during solution treatment. Mater Sci Eng. 2015;621:8-17.
13. Wang Z, Li M, Han Q, Yun X, Zhou K, Gardner L, et al. Structural fire behavior of aluminium alloy structures: review and outlook. Eng Struct. 2022;268:114746.
14. Jiang L, Wang C, Fu H, Shen J, Zhang Z, Xie J. Discovery of aluminum alloys with ultra-strength and high-toughness via a property-oriented design strategy. J Mater Sci Technol. 2022;98:33-43.
15. Taylor D. The theory of critical distances applied to the prediction of brittle fracture in metallic materials. Tech Sci Press. 2005;1(2):145-54.
16. Neuber H. Theory of notch stresses: principles for exact calculation of strength with reference to structural form and material. Berlin: Springer Verlag; 1958.
17. Peterson RE. Notch sensivity. In: Sines G, Waisman JL. editors. Metal fatigue. New York: McGraw Hill; 1959.
18. ASTM: American Society for Testing and Materials. ASTM B918: standard practice for heat treatment of wrought aluminum alloys. West Conshohocken: ASTM; 2017.
19. ASTM: American Society for Testing and Materials. ASTM E8: standard test methods for tension testing of metallic materials. West Conshohocken: ASTM; 2016.
20. Creager M, Paris PC. Elastic field equations for blunt cracks with reference to stress corrosion cracking. Int J Fract Mech. 1967;3:247-52.
21. Susmel L, Taylor D. The Theory of Critical Distances as an alternative experimental strategy for the determination of KIc and ΔKth. Eng Fract Mech. 2010;77(9):1492-1501.
22. ASTM: American Society for Testing and Materials. ASTM B221: standard specification for aluminum and aluminum-alloy extruded bars, rods, wier, profiles, and tubes. West Conshohocken: ASTM; 2014.
23. Callister WD Jr. Ciência e engenharia de materiais: uma introdução. 7. ed. Rio de Janeiro: LTC; 2008.
24. Farahmand B. Fatigue and fracture mechanics of high-risk parts: application of LEFM and FMDM theory. USA: ITP; 1997.
25. Tada H, Irwin G, Paris P. The stress analysis of cracks handbook. New York: ASME Press; 2000.